RSC Advances

ROYAL SOCIETY OF CHEMISTRY

www.rsc.org/advances

Tensile mechanical properties of Ni_3Al nanowires at intermediate temperature

Jingui Yu [a], Qiaoxin Zhang [a,*], Zhufeng Yue [b]

[a] School of Mechanical and Electronic Engineering, Wuhan University of Technology, Wuhan 430070, PR China

[b] Department of Engineering Mechanics, Northwestern Polytechnical University, Xi'an 710072, PR China

*Address correspondence to Q.X. Zhang

E-mail: zhangqx@whut.edu.cn (Q.X.Z)

Abstract

Molecular dynamics (MD) methods are employed to study the mechanical properties of Ni_3Al nanowires (NWs) along [001], [110] and [111] crystal orientations under tensile loading at intermediate temperature. The stress–strain responses, Young's modulus, elongations and crystal defects of NWs are compared at different temperatures with the different crystal orientations. The simulation results indicate that the yield stress decreases linearly with the increase of temperature, which is the same as the Young's modulus. In addition, tensile tests exhibit that the Ni_3Al NWs has an obvious intermediate temperature brittleness (ITB) behavior at about 900-1100 K. The crystal structure is less stable at intermediate temperature. Furthermore, we also find that the evolutions of different crystal defects are mainly point dislocations and stacking faults. The higher stacking fault energy (SFE) of Ni_3Al NWs, the easier dislocation slips. The glide dislocation expands within the {111} glide plane. Generally, studying the relation between the incipient plastic deformation and the temperature of Ni_3Al NWs under different crystal orientations can help us further understand the mechanical properties accurately and completely.

Keywords : Ni_3Al nanowires; Intermediate temperature; Crystal orientation; Molecular dynamics

1. Introduction

Ni_3Al is an intermetallic alloy with the face-centered-cubic $L1_2$ structure.[1] It has been intensively studied due to its potential high strength, high corrosion resistance and high thermal properties in the aerospace industry,[2-5] but it has been vexed with inherent crystallography characters limitations, especially the intermediate temperature (900-1100 K) brittleness (ITB).[6,7] Low plasticity, occurring at the intermediate temperature, limits the production, processing and application of Ni_3Al alloy.[1,8] For this reason, it's essential to have a well understanding of the mechanical properties in elastic and plastic deformation at intermediate temperature.

It is well accepted that the brittleness of Ni_3Al involve both intrinsic factors such as the existence of microcavities and extrinsic factors such as hydrogen embrittlement.[9] A great deal of experimental and theoretical effort has been made to elucidate the structural and mechanical properties. Recent studies have revealed that polycrystalline Ni_3Al suffers from severe intergranular brittleness at ambient temperatures, even though single crystals of Ni_3Al are quite ductile and extensive plasticity can be observed on the intergranular fracture surface.[10] Furthermore, though a few investigators suggested that temperature significantly affected the mechanical properties of singlephase Ni_3Al,[11-13] tensile tests of multiphase Ni_3Al-based alloys have been conducted primarily at room temperature.[14] However, the research works on the mechanical properties of NWs have mainly relied on atomistic simulations instead of experiments. MD simulations have been utilized to evaluate the properties of the NWs and explain the fundamental mechanisms in the process of the mechanical

deformation in a form of numerical experiments to compliment studies in laboratories[15]. Setoodeh et al.[16,17] simulated the mechanical properties of nickel NWs at different temperatures (temperature varies between 50 K and 600 K). Tschopp and McDowell used atomistic simulations to investigate how the stress required for homogeneous nucleation of partial dislocations in single crystal copper under uniaxial loading changes as a function of crystallographic orientation.[18,19] Gao et al. employed the embedded-atom method (EAM) potential to study anisotropic and temperature effects on mechanical properties of copper NWs under tensile loading.[20] Alavi et al. studied mechanical properties of Ni-Al NWs by calculating the stress–strain response of the wires under various loading conditions.[15] In addition, Huang et al. simulated the uniaxial tensile deformation of FCC nickel NWs and observed the strain rate and size effects on mechanical properties.[21] However, previous studies are focused on the lower temperature mechanical properties of NWs from 10 K to 700 K，no model has yet been proposed to investigate the mechanical properties of Ni_3Al NWs under tensile loading at intermediate temperature.

The purpose of this study is to perform the MD simulations with EAM to investigate the temperature and anisotropic effect on mechanical properties of Ni_3Al NWs by reporting the stress–strain responses, Young's modulus, elongation and crystal defects. The elongation was followed by a particular discussion on ITB of NWs from the standpoint of the content of stacking faults. A deep understanding to the plasticity of Ni_3Al NWs under tensile loading was achieved.

2. Simulation methods

Here MD simulations with EAM potential were performed to study the mechanical properties of Ni_3Al NWs under the uniaxial strain along different crystal orientations ([001], [110], [111]). The EAM had been proposed by Yamakov, [22] Daw and Baskes[23] as a numerical method for calculating atomic energetics. It had been widely used for deformation research of the nickel NWs.[15,16] In the EAM，the total energy E_{pot} of a system of N atoms can be written as

$$E_{pot} = \sum_{i=1}^{N} (F_i(\rho_i) + \frac{1}{2}\sum_{j \neq i} \phi_{ij}(r_{ij}))$$

$$\rho_i = \sum_{j \neq i} \rho_{ij}^{a}(r_{ij})$$

where F_i is the embedding energy of atom *i*, ρ_i is the electron density at site *i*, ϕ_{ij} is the pair potential function between atoms *i* and *j* and ρ_{ij}^{a} is the atomic charge density of atom j at the location of atom *i*.

The crystal was in the cubic orientation. Periodic boundary conditions were prescribed in all three orthogonal directions. The simulation was carried out by integrating Newton's equations of motion for all atoms using a time step of 1 fs. At the start of simulation, The Ni_3Al NWs was then minimized based the aforementioned EAM interatomic potentials. Samples are relaxed using molecular dynamics for 100 ps at 100 K. This configuration were then heated to different temperatures (800-1200 K) and used as a starting configuration in the molecular statics technique to study the mechanical properties of Ni_3Al NWs. Two layer atoms at the most bottom and top are fixed as a plane in the model. And displacement with a movement rate 1.5 Å/ps was applied to the top plane which was a reasonable value for MD tension simulations. The MD simulations were carried out as a NPT isothermal isobaric ensemble. For convenience of comparison, almost the same size were selected in the three different models of our simulations. The open source MD code LAMMPS[24] and the visualization tools AtomEye[25] were used in the atomistic simulations. The stresses are calculated using the virial theorem.

The elements of the tensor of atomic-level stresses were calculated as

$$\sigma_{\alpha\beta}(i) = -\frac{1}{2\Omega}\left[\sum_j F_{ij}^{\alpha} r_{ij}^{\beta} + 2M_i v_i^{\alpha} v_i^{\beta}\right]$$

where α and β label the Cartesian components, Ω is the atomic volume, F_{ij} is the force on atom i due to atom j , M_i is the mass of atom i, and v_i is the velocity of atom i. An effective stress (σ_e) and an effective strain (ε_e) according to the von Mises criterion for yielding was calculated as

$$\sigma_e = \left[\left(\left(\sigma_x - \sigma_y\right)^2 + \left(\sigma_y - \sigma_z\right)^2 + \left(\sigma_z - \sigma_x\right)^2 + 6\left(\sigma_{xy}^2 + \sigma_{xz}^2 + \sigma_{yz}^2\right)\right)/2\right]^{1/2}$$

$$\varepsilon_e = \frac{1}{3}\left[2\left(\left(\varepsilon_x - \varepsilon_y\right)^2 + \left(\varepsilon_x - \varepsilon_z\right)^2 + \left(\varepsilon_y - \varepsilon_z\right)^2\right)\right]^{1/2}$$

where σ_x, σ_y, and σ_z are the stresses averaged over the entire system in the X, Y, and Z directions, respectively, and ε_x, ε_y, and ε_z are the engineering strains in the X, Y , and Z directions, respectively.[26,27]

We performed uniaxial tensile MD simulations on the three atomic models: [001] crystal orientation, [110] crystal orientation, and [111] crystal orientation, as shown in Table 1. In solid-state systems, centro-symmetry parameter (CSP) is a useful measure of the local lattice disorder around an atom and can be used to characterize whether the atom is part of a perfect lattice, a local defect, or a free surface.[28] In order to clearly visualize the defects, the CSP for each atom in the system except the fixed plane atoms is calculated. The CSP is defined as follows:

$$CSP = \sum_{i=1}^{N/2} \left| \vec{R}_i + \vec{R}_{i+N/2} \right|^2 ,$$

where the N are the number of neighbors for each atom. $\vec{R}_i$ and $\vec{R}_{i+N/2}$ are the vectors or bonds corresponding the $N/2$ pairs of opposite nearest neighbors in the

system.

3. Results and discussion

3.1. Deformation behavior under tensile loading

Fig.1 presents the stress–strain relationships of NWs along three different crystal orientations at different temperatures. The yield stress of NW in [001] crystal orientation at room temperature (300 K) is greater than the yield stress at intermediate temperature, as shown in Fig.1(a). The yield stress decreases from 0.3445 GPa to 0.247 GPa as the temperature gradually increasing from 300 K to 1200 K. Ni_3Al NWs show good elastic performance before yield, and the stress-strain relationships follow a linear Hooke's law. At plastic stage, the stress-strain curve fluctuates at 800 K, which indicates that NW has a small range of work hardening. The yield stress of Ni_3Al NW decreases obviously at 1100 K. Compared with Fig. 1(a),the temperature has a little effect on yield stress in Fig. 1(b). The yield stress of 1200 K is about 26.0% smaller than the Ni_3Al NWs at 300 K. At plastic stage, the stress-strain curve fluctuates significantly, and the stress increases with strain, which indicates that the work hardening in [110] crystal orientation is more evident than in [001] crystal orientation. The stress-strain curves are similar in Fig. 1(c) and Fig. 1(a). The yield stress of [001] crystal orientation is larger than the yield stress of [111] crystal orientation at the same temperature. The yieldings of three different types of Ni_3Al NWs are accommodated by the activities of Shockley partial dislocations.[29] Results show that the stress-strain responses are strongly dependent on NW's orientation and temperature.

There is a fine linear relationship between the yield stress and the temperature in different crystal orientations, as shown in Fig.2. The yield stress changes slowly with the increasing temperature in [110] crystal orientation. However, the yield stresses decline significantly in [001] crystal orientation and [111] crystal orientation. In [110] crystal orientation, the yield stress decreases by 26.0% compared with 30.7% in [001] crystal orientation and 45.6% in [001] crystal orientation with increasing temperature (from 300 K to 1200 K). At higher temperature, the atomic structure has high entropy, and the atoms vibrate around their equilibrium position with much larger amplitude, as compared to those at low temperatures.[30]

As mentioned, the temperature has a great influence on the mechanical properties of Ni_3Al NW. the declining rate of yield stress is shown to have $\sigma_{[111]} > \sigma_{[001]} > \sigma_{[110]}$ for Ni_3Al NWs. The work hardening in [110] crystal orientation is more evident than in [001] crystal orientation, and the [111] crystal orientation hardly has a work hardening effect. This is mainly because that with the plastic deformation of Ni_3Al NWs, the grain crystals slip and appear dislocation tangles, in the end crystal grains elongate and destruct. This results in the increase in strength and hardness but the decrease in ductility and toughness of Ni_3Al NWs. The results accord with other reported.[31-33] Although the structure of Ni_3Al is simpler than nickel-base single crystal, this simulation will provide the theoretical basis for the further study of the mechanical properties of Ni_3Al NWs in different crystal orientations at intermediate temperature.

The simulation results of Yield stress results consistent with previous report.[34-36] However, the yield stress in reference is greater than the analog value at the same

temperature. There are several reasons that can account for this fact, but the following four may be the main ones. First, our study is on Ni_3Al NWs and Ni-based superalloys are strengthened by fine and ordered γ' precipitates embedded in an FCC γ matrix. These alloys are far stronger than pure γ or γ' single phase materials due to the presence of γ/γ' interfaces which prevents dislocation motion at high temperatures.[37] But making use of the Ni_3Al nanowires to study the ITB is feasible because Ni_3Al is the main component of γ 'phase, and it has similar mechanical properties to Ni-based superalloys. Second, we take a small strain rate 2×10^9. The higher the strain rate, the lager the corresponding yield stress changes.[38] In addition, size effect is an important factor that affect the yield stress.[39] The larger size of Ni_3Al NWs, the higher yield stress at micro and nano scale. Last and most important, Nickel-based alloys generally contain Co, Cr and other elements. Alloy elements greatly improve the mechanical properties of Ni_3Al NWs.[34,35]

The Young's modulus is defined as the first derivative of the stress with respect to the strain at the equilibrium state by the following equation:

$$E = \left(\frac{d\sigma}{d\varepsilon}\right)_{\varepsilon=0}$$

where ε is the strain.[40] Fig.3 depicts the variations of Young's modulus of the Ni_3Al NWs at various temperatures. The Young's modulus deceases nearly linearly with the increasing temperature. In [001] crystal orientation, the Young's modulus at 1200 K is about 32.6% smaller than at 300 K compared with 41.4% in [110] crystal orientation and 34.98% in [111] crystal orientation. The Young's modulus increases with the increasing temperature from 1000 K to 1100 K, while it decreases evidently with increasing temperature from 1100 K to 1200 K in [111] crystal orientation. Then the

conclusion can be drawn that Young's modulus of the NWs has a negative temperature coefficient, which is in agreement with the experimental results.[7,41,42] It is noted that the calculated Young's modulus at 900-1200 K are closer to experimental measurements. Considering that there are some defects or impurities in Ni_3Al NWs prepared experimentally and they could weaken the elastic modulus of Ni_3Al NWs, our calculated Young's modulus is corresponding with the experimental results. The different values may due to the different definitions about elastic constants and crystal orientation. The trend of the Ni_3Al NW's elastic property is in accord with many other materials like Nickel NW[16] and Ni-Al NW.[15] Furthermore, the simulation results correspond well with the results of Gao.[20] These phenomena can be illustrated as follows. The equilibrium distance between two particles (r) corresponds to a minimum potential energy. In addition, a simple analysis of bonding force shows that the Young's modulus is proportional to ($1/r^n$).Therefore by increasing the temperature, the equilibrium distance of the particle separation is increased.[16] This induces the decline of Young's modulus. Therefore, both the variation of stress–strain curves and the drop of Young's modulus indicate the less stable crystal structure as increasing of temperature.[20,43] With temperature ranging from 300 K to 500 K, the Young's modulus of [110] crystal orientation is greater than the value in [001] crystal orientation. The Young's modulus is shown to have $E_{[111]} > E_{[001]} > E_{[110]}$ at the same temperature. The reason might be the difference of the equilibrium distance, as shown in Table 1. Therefore, the Young's modulus decreases through the increase of the equilibrium distance.

Elongation (δ) is a description index of the plastic performance. It is the ratio of the extension in length of the specimen after fracture to its initial gauge length, expressed in percent.

$$\delta = \frac{(l_1 - l_g)}{l_1} \times 100\%$$

where l_1 is gauge length of specimen after fracture, l_g is gauge length before fracture(i.e. initial gauge length)

In [001] and [111] crystal orientations, the elongation percentages of Ni_3Al NWs dramatically decline at 900 K, as shown in Fig. 4, there is an ITB phenomenon when the temperature ranges from 800 K to 1100 K. Meanwhile, in [110] crystal orientation, the change of the elongation percentage is not clear, but the fluctuation is obvious. However, it still shows that the Ni_3Al NW has an ITB behavior. The changing trend of elongation percentage between 300 K and 900 K is the same as the strength, while in the other temperatures, the changes are almost inverse. What is interesting is that the elongation percentage declines slightly after 800 K and then rises significantly after 1100 K. These agree with the experimental results.[3,7,44]

3.2. Evolution of different crystal defects

The pink lines represent the fraction of surface steps, as shown in Fig. 5. We can see that the fraction of surface steps and perfect surfaces are barely changed, the content of surface steps and perfect surfaces are relatively low in all disordered atoms due to the limited dimensions of the system. This will lead to the happening of necking in tension process. The fraction of all dislocations and stacking faults change

clearly after yielding. These results are closely consistent with the foregoing description of Fig.1 and Fig.2.

The value of CSP for all dislocations of systems is greater than 1, stacking faults greater than 4 and less than 11, point dislocations greater than 1 and less than 4, perfect surface greater than 11 and less than 19 and surface step greater than 19. Evolution of different crystal defects are mainly point dislocations and stacking faults. The influence of different crystal orientations on the evolution of point dislocations and stacking faults is [110] > [111] > [001]. Meanwhile, this can also explain how difficult the open slip system of Ni_3Al NW is in different crystal orientations. To further understand the different yield responses of the NWs at 900 K, lateral view of the Ni_3Al NWs dislocations snapshots are shown in Fig. 6.

Fig. 7 shows the evolution of different crystal defects at 800 K and 1000 K. The higher the temperature, the greater proportion of point dislocations and stacking faults at the same strain. Although the surface steps and perfect surfaces are basically horizontal lines, and these do not mean that no necking occurs in NWs. Necking forms in the center of the NWs and extends to the border. The shape of the NW is extremely uneven which is not due to the content of surface steps and the fraction of perfect surfaces.

To further understand the influence of temperature on the evolution of stacking faults, front view of the Ni_3Al NWs stacking faults snapshots are shown in Fig. 8. In [110] crystal orientation, the temperature significantly affects the content of stacking faults. The SFE is proportional to the temperature,[45] as shown in Table 2. Meanwhile,

the higher SFE of Ni_3Al NWs, the easier dislocation slips. In addition, comparing Fig.8 with Fig.2, the yield stress of Ni_3Al NWs decreases with the increase of SFE. The glide dislocation is nucleated from the ends of NWs, and it expands within the {111} glide plane.[43] Finally, the forest interactions directly form the sessile dislocations. Glide dislocations emits mainly in both [101] and [$\bar{1}$01] directions.

The energy variation of the supercell after introducing stacking fault is

$$\Delta E_{SF} = E_{SF} - E_0$$

where E_0 is the total energy of the perfect crystal, and E_{SF} is the total energy of the crystal with stacking fault structure. The stacking fault energy is defined as

$$\gamma_{SF} = \Delta E_{SF} / \Delta S$$

where ΔS is the area of stacking fault in the supercell.[46]

With the increasing temperature, the thermal motion of molecules will be more violent and the interatomic distance will be expanded, furthermore the atomic diameter and lattice constants will also change. The above changes will lead to the increasing SFE.[47,48] When SFE is high, dislocation can extend or tangle easily, then the work hardening of Ni_3Al NWs lags and vice versa.

4. Conclusion

In conclusion, MD simulation has been performed to study the influence of different crystal orientations and temperatures on the mechanical properties of Ni_3Al NWs under tensile loading. The results show that the crystal orientation and temperature play an important influence on yield stress, Young's modulus and ITB behavior of Ni_3Al NWs. The yield stress of NW has a significant linear correlation

with the temperature in different crystal orientation. The yield stress changes slowly with increasing temperature in [110] crystal orientation, and declines significantly in [001] crystal orientation and [111] crystal orientation. The difference of Young's modulus is shown as $E_{[111]} > E_{[001]} > E_{[110]}$ for Ni_3Al NWs. In addition, ITB phenomenon is distinct at 800 K to 1100 K. Furthermore, we also find that evolution of different crystal defects are mainly point dislocations and stacking faults. The higher SFE of Ni_3Al NWs, the easier dislocation slips. The glide dislocation expands within the {111} glide plane.

Acknowledgements

This work was supported by the National Natural Science Foundation of China (No. 51210008).

References

1 J. Wang, Y.W. Chung, Intermetallics, 2001, **9**, 349.
2 Y. Li, J. Zhao, G. Zeng and C. Guan, Mater Lett, 2004, **58**, 1629.
3 G.X. Yang, Y.F. Xu, L. Jiang and S.h. Liang, Prog Nat Sci Mater,2011, **21**, 418.
4 D. Cheng, S. Wang, C. Wang and Z. Wang, Mod Phys Lett B, 2010, **24**, 1639.
5 H. Yu, Y. Su, N. Tian and S. Tian, Mat Sci Eng A. 2013, **565**, 292.
6 C. Yuan, X. Sun, F. Yin and H. Guan, J Mater Sci Technol. 2001, **17**, 425.
7 L.Z. He, Q. Zheng, X.F. Sun and G.C. Hou, Mat Sci Eng A. 2004, **380**, 340.
8 T.M. Pollock, S. Tin, J Propul Power. 2006, **22**, 361.
9 J.Q. Su, M. Demura, T. Hirano, Acta Mater. 2003,**51**, 2505.
10 G.W. Han, C.S. Lee, D. Feng and J.K.L. Lai, Scripta Mater. 1998, **38**, 653.
11 W. Xu, X.Meng, C. Yuan and A. Ngan, Mater Lett. 2000, **46**, 303.
12 J. Adamiec, Adv Mater Sci Eng. 28 (2007) 333-336.
13 E. George, C. Liu, D. Pope, Acta mater. 1996, **44**, 1757.
14S.A.Sajjadi,S.M.Zebarjad,Journal of Achievements in Materials and Manufacturing Engineering. 2006, **18**,1.

15 A. Alavi,K. Mirabbaszadeh, P. Nayebi and E. Zaminpayma, Comp Mater Sci,2010, **50**, 10.

16 A.R. Setoodeh, H. Attariani and M. Khosrownejad, Comp Mater Sci,2008,**44**,378.

17 A.R. Setoodeh, H. Attariani, Mater Lett, 2008, **62**, 4266.

18 M.A. Tschopp, D.E. Spearot and D.L. McDowell, Model Simul Mater Sc,2007, **15**, 693.

19 M.A. Tschopp, D.L. McDowell, J Mech Phys Solids, 2008, **56**, 1806.

20 Y. Gao, H. Wang, J. Zhao and C. Sun, Comp Mater Sci, 2011, **50**, 3032.

21 D. Huang, Q. Zhang and P. Qiao, Comp Mater Sci, 2011, **50**, 903.

22 V. Yamakov, D. Wolf, S. Phillpot and H. Gleiter, Acta mater, 2002, **50**, 61.

23 M. Daw, M. Baskes, Phys Rev B, 1984, **29**, 6443.

24 S. Plimpton, J Comput Phys, 1995, **117**, 9.

25 J. Li, Model Simul Mater Sc, 2003,**1**, 173.

26 Dongare A M, Rajendran A M and LaMattina B, Comp Mater Sci, 2010, **49**, 260.

27Dongare A M, LaMattina B and Rajendran A M, J Eng Mater-T, 2012, **4**,134.

28 C.L. Kelchner, S. Plimpton and J. Hamilton, Phys Rev B, 1998, **58**, 11085.

29 Y.H. Wen, Y. Zhang, Q. Wang and J.C. Zheng,Comp Mater Sci. 2010,**48**, 513.

30 W.X. Wang, L.S. Niu, Y.Y. Zhang and E.Q. Lin, Comp Mater Sci, 2012, **62**, 195.

31 H. Honjo, Y. Kaneno, H. Inoue and T. Takasugi, J Mater Sci, 2004, **39**, 3677.

32 Z. Lian, J. Yu, X. Sun and H. Guan, Mat Sci Eng A. 2008, **489**,227.

33 D. Lee, M.L. Santella, Mat Sci Eng A, 2006, **428**, 196.

34 S. A.Sajjadi, S. Nategh and RI L.Guthrie, Mat Sci Eng A-Struct, 2002, **325(1)**, 484.

35 T. M. Pollock, S.Tin, J Propul Power, 2006, **22(2)**, 361.

36 C. J. Tong, Y. L. Chen and J. W. Yeh, Metall Mater Trans A, 2005, **36(4)**,881.

37 W. P. Wu, Y. F. Guo and Y. S. Wang, Phil Mag, 2011, **91(3)**, 357.

38 Huang, Zhang Q and Qiao P, Comp Mater Sci, 2011, **50(3)**, 903.

39 Dongare A M, Rajendran A M and LaMattina B, Comp Mater Sci, 2010,**49(2)**,260.

40 Wen Y H, Zhang Y and Wang Q, Comp Mater Sci,2010, **48(3)**,513.

41R.Srinivasan, M.S.Daw, R.D. Noebe and M.J. Mills, Philos Mag, 2003,**83**, 1111.

42 M. Eskner, R. Sandström, Surf Coat Tech, 2003, **165**, 71.

43 Q.N. Guo, X.D. Yue, S. E. Yang and Y.P. Huo, Comp Mater Sci, 2010, **50**, 319.

44 J. Wang, J. Qian, X. Zhang and Y. Wang, Rare Metals, 2011, **30**, 422.

45X.F.Yu,S.G.Tian and M.G.Wang, Chinese Journal of Materials Research,2008, **22(5)**,515.

46Y.F.WEN, J.SUN and J.HUANG, Trans. Nonferrous Met. Soc. China 2012,**22**, 661.

47 D. G. Pettifor, Mater Sci Tech-Lond, 1992, **8(4)**, 345.

48 Y.Mishin, Acta Mater, 2004, **52(6)**,1451.

Figure captions

Fig. 1. Stress-strain curves for different crystal orientations NWs at different temperatures.

Fig. 2. The yield stress of Ni_3Al NWs at different temperatures with different crystal orientations.

Fig. 3. The Young's modulus of Ni_3Al NWs at different temperatures with different crystal orientations.

Fig. 4. Temperature dependence of the elongation percentage of Ni_3Al NWs with three different crystal orientations.

Fig. 5. Evolution of different crystal defects at different crystal orientations (T= 900 K). (a) represents the situation of [001] crystal orientation. (b) represents the situation of [110] crystal orientation. (c) represents the situation of [111] crystal orientation.

Fig. 6. Snapshots of lateral views for the evolution of stacking faults in different crystal orientations at 900 K. The atoms are colored by CSP values.

Fig. 7. Evolution of different crystal defects in [001] crystal orientation. (a) represents the situation of 800 K. (b) represents the situation of 1000 K.

Fig.8. Snapshots of front views for the evolution of stacking faults at different temperatures in [110] crystal orientation. The atoms are colored by CSP values.

Table caption

Table 1. Atomic configurations for the three models: [001] crystal orientation, [110] crystal orientation, and [111] crystal orientation.

Table 2. Stacking fault energy of Ni_3Al NWs at different temperatures in [110] crystal orientation.

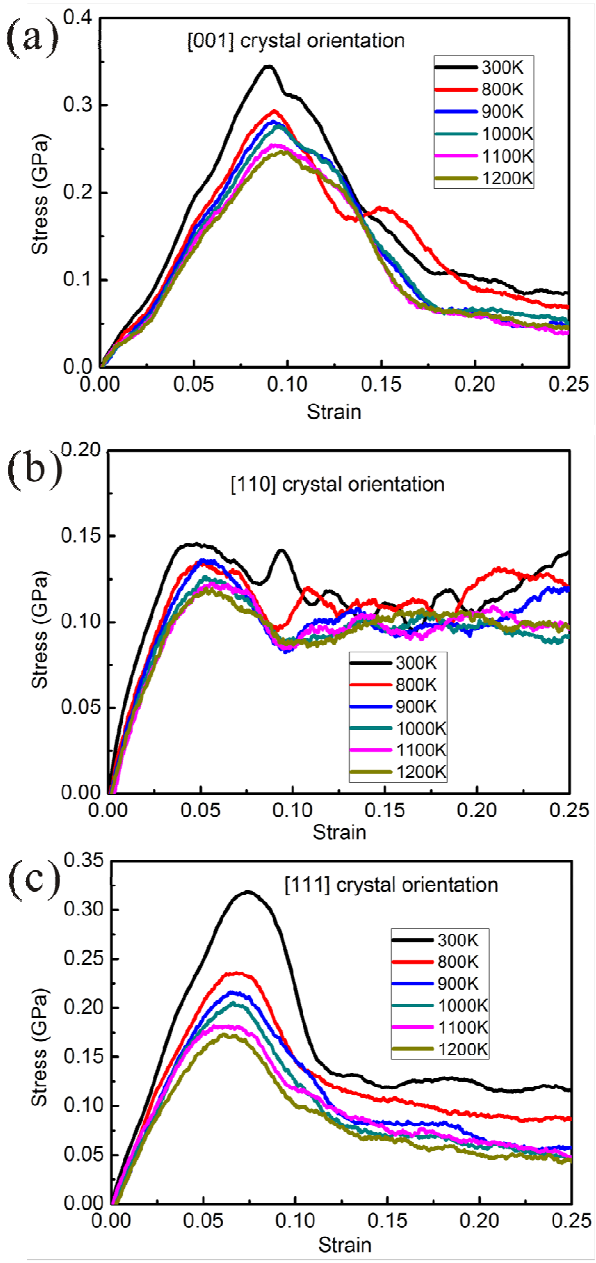

Fig. 1

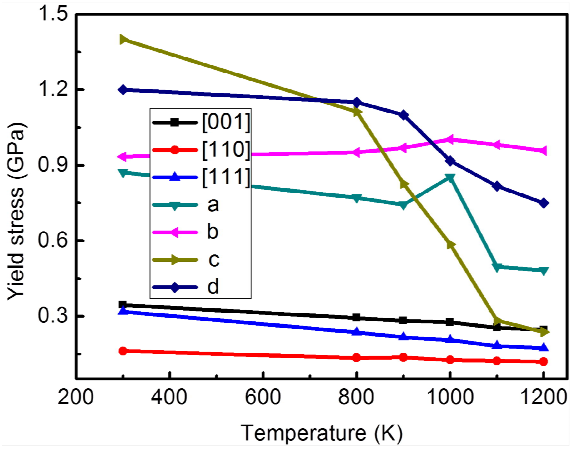

Fig. 2

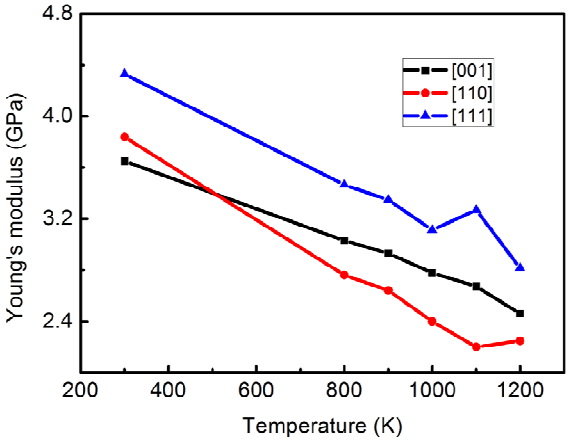

Fig. 3

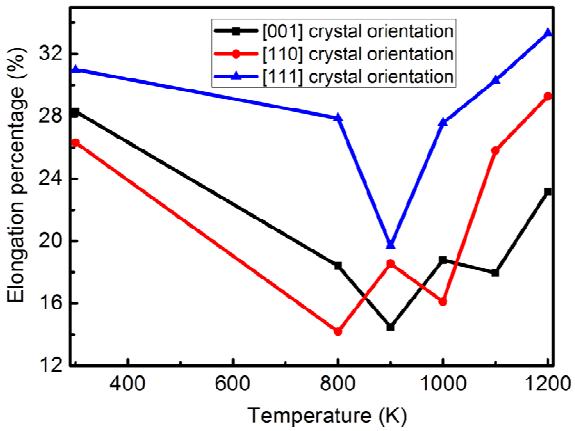

Fig. 4

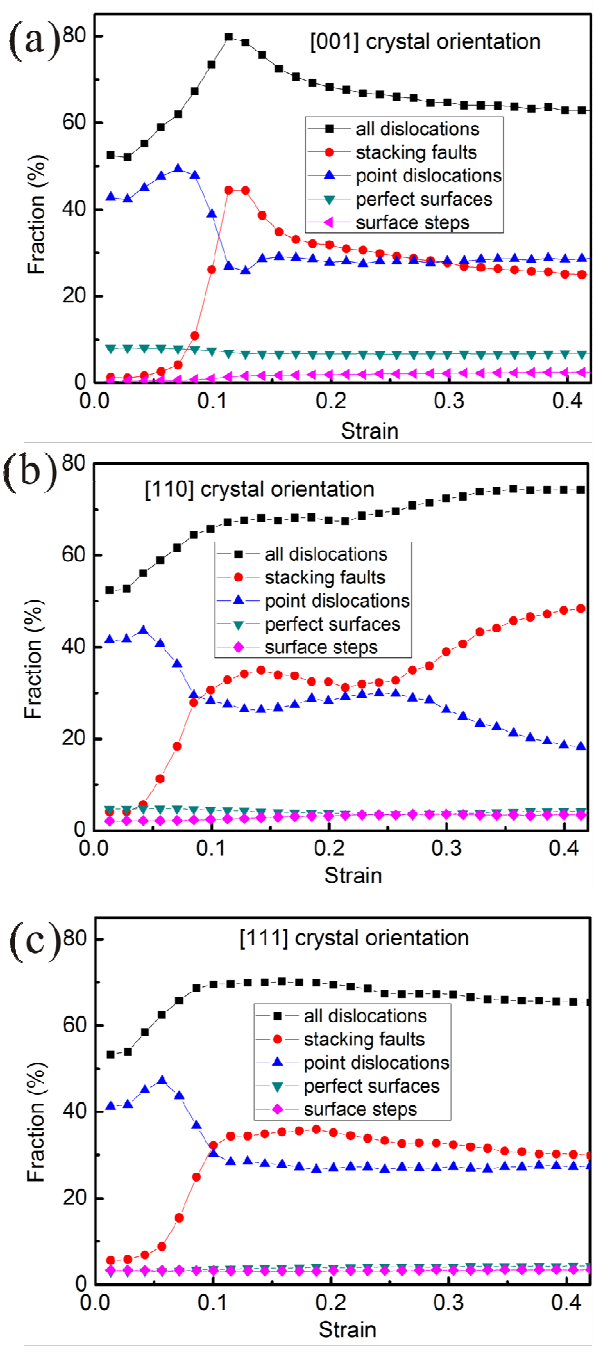

Fig. 5

Crystal orientations	2.857 %	5.714 %	9.962 %
[001]	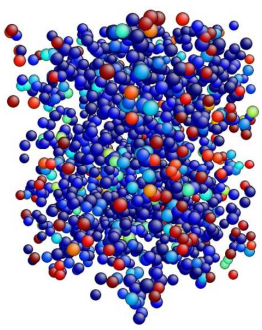 (a)	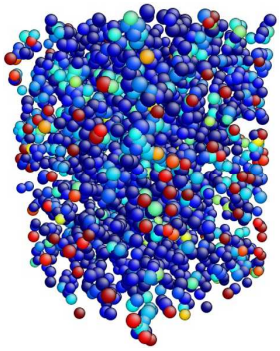 (b)	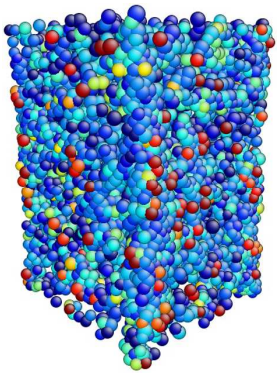 (c)
[110]	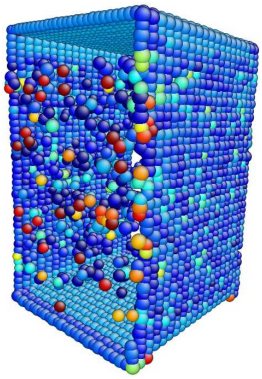 (a')	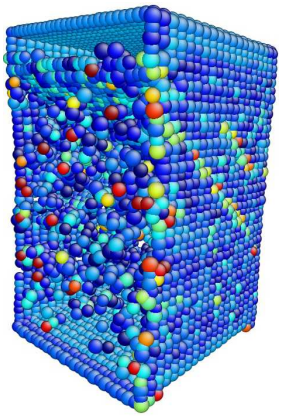 (b')	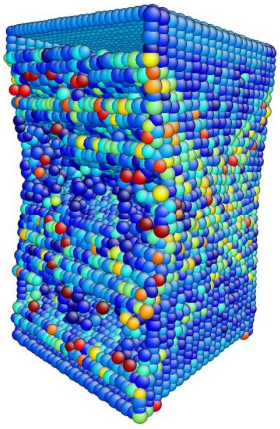 (c')
[111]	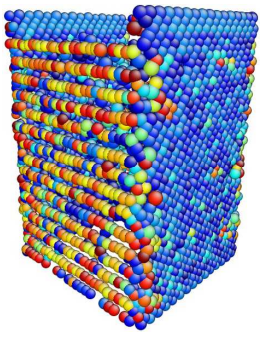 (e)	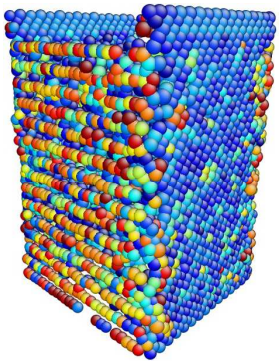 (f)	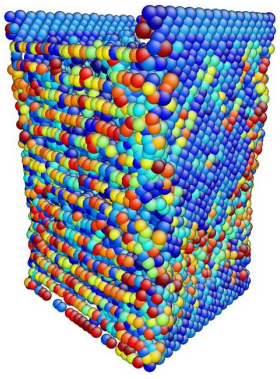 (g)

Fig. 6

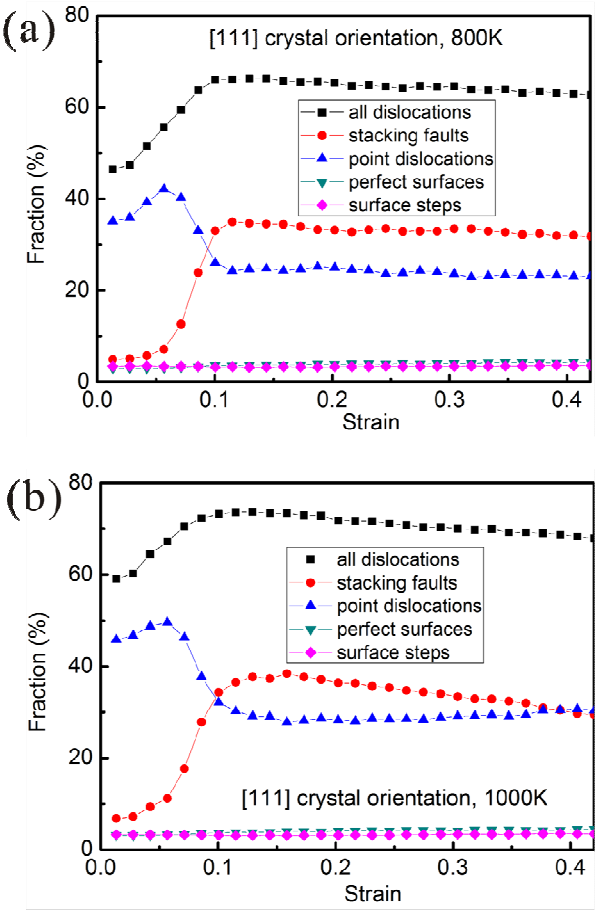

Fig. 7

Temperature	800 K	900 K	1000 K	1100 K
[110] crystal orientation ε =7.212%	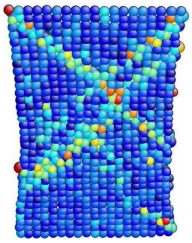 (a)	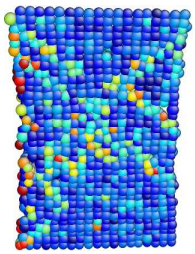 (b)	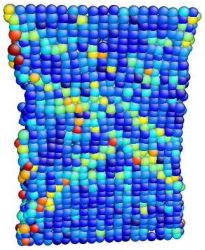 (c)	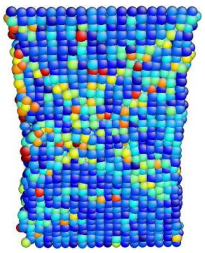 (d)

Fig. 8

Table 1

Crystal orientations (x, y, z)	Lattice constants (a×b×c)	Number of atoms	Model sizes
[100], [010], [001]	3.573Å×3.573Å×3.573Å	48000	20a×20b×30c
[$\bar{1}$10], [001], [110]	5.053Å×3.573Å×5.053Å	47040	14a×20b×21c
[11$\bar{2}$], [$\bar{1}$10], [111]	8.752Å×5.053Å×6.189Å	45696	8a×14b×17c

Table 2

Temperature	800 K	900 K	1000 K	1100 K
SFE (mJ/m^2)	252.54	269.32	276.61	280.56
Ref.a,b,c (mJ/m^2)	290.15[a]	305.39[a]	337.22[b]	260[c]

[a]Ref. 45, [b]Ref. 46, [c]Ref. 47.